Opto-Electronic Science

Supplementary information

February 2025, Vol. 4, No. 2

DOI: 10.29026/oes.2025.240021 CSTR: 32246.14.oes.2025.240021

Enhanced amplified spontaneous emission via splitted strong coupling mode in large-area plasmonic cone lattices

Jiazhi Yuan[1†], Jiang Hu[1†], Yan Zheng[1,3,4*], Hao Wei[1,3], Jiamin Xiao[1], Yi Wang[1,2], Xuchao Zhao[1], Ye Xiang[1], Yong Lei[4*] and Wenxin Wang[1,2,5*]

[1]Qingdao Innovation and Development Center of Harbin Engineering University, Harbin Engineering University, Qingdao 266500, China; [2]College of Physics and Optoelectronic Engineering, Harbin Engineering University, Harbin 150001, China; [3]College of Material Sciences and Chemical Engineering, Harbin Engineering University, Harbin 150001, China; [4]Institute of Physics, Department of Mathematics and Natural Sciences, TU Ilmenau, Ilmenau 98693, Germany; [5]College for Advanced Interdisciplinary Studies, National University of Defense Technology, Changsha 410073, China .

[†]These authors contributed equally to this work.

*Correspondence: Y Zheng, Email: yan.zheng@hrbeu.edu.cn; Y Lei, Email: yong.lei@tu-ilmenau.de;
WX Wang, E-mail: wenxin.wang@hrbeu.edu.cn

This file includes:

Supplementary information for this paper is available at https://doi.org/10.29026/oes.2025.240021

Section 1: Effect of anodic oxidation voltage on AAO

Figure S1 Demonstrates the morphological of PCLs at anodic oxidation voltages of 30 V, 40 V, and 50 V. Period of PCLs increases with increasing anodic oxidation voltage. During two-part anodic oxidation, AAO undergoes self-organizing into honeycomb arrangement which is short ordered[S1,S2]. $C_2O_4^{2-}$ as anion allows AAO to grow more uniformly. PCLs grows in a honeycomb arrangement which is affected by AAO membrane. Below are schematics of AAO growth at the cross-section. The thickness of wall (t_w) is affected by anodic oxidation voltage and the diameter of pore (d_p) is affected by anion concentration. The d_p is invariant for fixed anion concentration and no-nanoimprinting conditions, so the interpore distance (D_{int}) of AAO become larger. Al foil is controlled by AAO stress, so the period of PCLs becomes larger[S3].

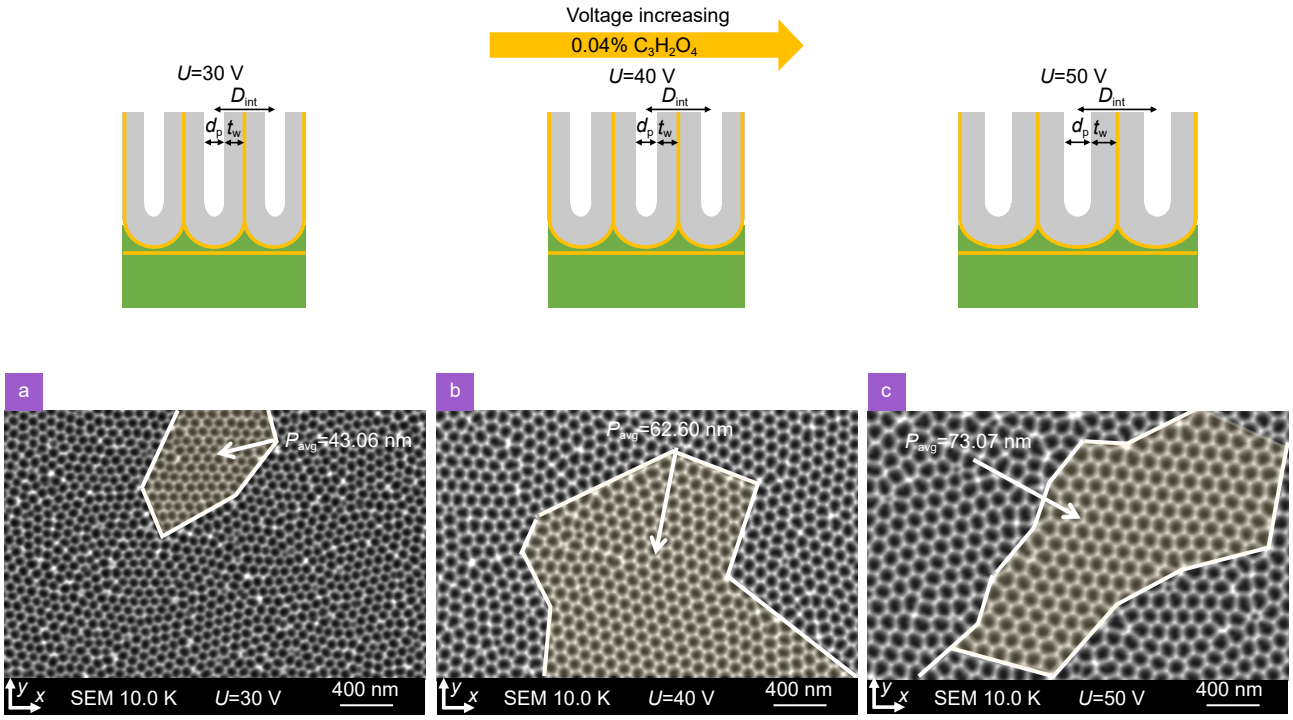

Fig. S1 | Demonstrating the effect of voltage for period of PCLs by using a two-step anodic oxidation. (**a**-**c**) shows topography of PCLs under different voltage conditions of anodic oxidation. $C_2O_4^{2-}$ with a mass fraction of 0.04 as anion. PCLs is positively correlated with the anodic oxidation voltage (When anodic oxidation voltages are 40 V, 50 V, and 60 V, the PCLs period are 43.06 nm, 62.60 nm, 73.07 nm, respectively). The cross-section schematics of PCLs are shown on above. With the anodic oxidation voltage increases, the expansion on horizon of AAO becomes larger.

Section 2: Measurement system

An angle-resolved spectrum system is used to measure the ASE of Nile Red based on Bloch-SPPs and LSPs mode supported by the PCLs. As shown in the schematic optical path of Fig. S2, a 532 nm solid-state laser serves as the pump source to excite Nile Red with a power density of 219 W/cm². The incident angle θ_{in} and the emission angle θ_{em} are consistent with the same plane.

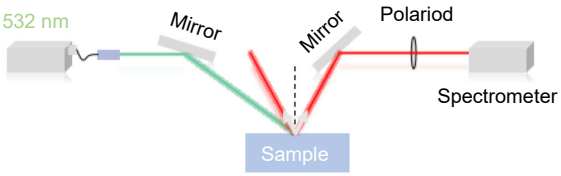

Fig. S2 | Angular resolution optical path diagram for the measurement of ASE.

Section 3: Schematic diagram of the energy levels transition and the energy transfer

To further illustrate the energy transfer between the optical cavity and the gain medium, the energy branch of UP and Nile Red are firstly explored. On one hand, the Bloch-SPPs mode facilitates rapid energy exchange with the LSPs mode near the cone tip. On the other hand, as a typical four energy level system, the energy level diagram of Nile Red is presented in Fig. S3. Electrons are excited from the S_0 to the S_3 state by the 532 nm laser, followed by non-radiative decay from S_3 to S_2. Spontaneous emission at 638 nm is then generated by the transition from S_2 to S_1. The main reason for the maximum ASE enhancement effect at 638 nm is that the band-edge UP mode has a higher density of localized states than other energy levels. The electric field enhancement at the UP facilitates particle number inversion between the S_2 and S_1 energy levels. Additionally, the photons generated by ASE are transferred to the metal surface, exciting the UP, which results in effective resonance feedback and optical amplification.

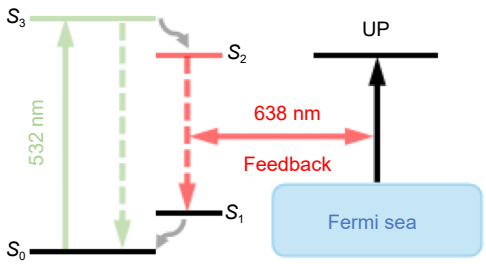

Fig. S3 | Schematic diagram of the energy levels transition and the energy transfer in the generation of ASE.

Section 4: Polarization dependence

The polarized emission of the ASE at 1.12 is investigated in Fig. S4 by comparing the polarized coherence radar map of the PCLs with that of the flat Al foil, at 638 nm. The ASE on the AAO exhibits elliptical polarization coherence and higher intensity at 0° and 90°, which is related to the lattice arrangement. The polarized emission of the ASE can be well fitted by a typical electric dipole resonance of the angular function (light red fitted line in Fig. S4). This function can be expressed as $A\cos^4(\delta - \delta_0) + B\cos^4(\delta - \delta_1)$, where δ is the angle of polarization and δ_0 and δ_1 are the two fitting constants. The fitting of an approximate 30° polarization on the Al foil illustrates the modulating effect of the PCLs on the laser field rather than the source itself carrying its own polarization information.

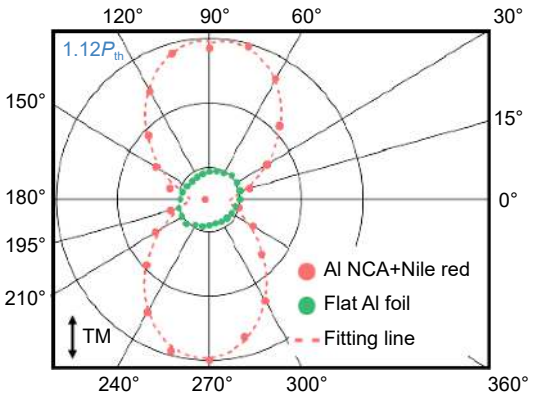

Fig. S4 | Polarization of ASE on PCLs and flat Al foil. TM polarization is 90°, while TE polarization is 0°.

Section 5: The full quantum mechanical model based on CQED for strong coupling system

The following is the full quantum mechanical model for the strong coupling system based on the cavity quantum electrodynamics (CQED), in which the Bloch-SPPs mode and LSPs mode are treated as bosonic modes. The Hamiltonian of the strong coupling system contains three parts:

$$\hat{H} = \hat{H}_{\text{Bloch-SPPs}} + \hat{H}_{\text{LSPs},l} + \hat{H}_{\text{I}} = \hbar\omega_{\text{Bloch-SPPs}}\hat{a}^{\dagger}\hat{a} + \sum \hbar\omega_{\text{LSPs},l}\hat{b}_{\text{l}}^{\dagger}\hat{b}_{\text{l}} + \sum \hbar g_{\text{l}}(\hat{a}^{\dagger} + \hat{a})(\hat{b}_{\text{l}}^{\dagger} + \hat{b}_{\text{l}}) \ , \tag{S1}$$

here, the first term $\hat{H}_{\text{Bloch-SPPs}} = \hbar\omega_{\text{Bloch-SPPs}}\hat{a}^{\dagger}\hat{a}$ is the Hamiltonian of Bloch-SPPs mode with frequency $\omega_{\text{Bloch-SPPs}}$, where $\hbar\omega_{\text{Bloch-SPPs}}$ is the photon energy of Bloch-SPPs mode, $\hbar$ is reduced Planck constant, $\hat{a}^{\dagger}$ and $\hat{b}_{\text{l}}^{\dagger}$ are the creation operator, and $\hat{a}$ are $\hat{b}_{\text{l}}$ annihilation operator. The second term $\hat{H}_{\text{LSPs},l} = \sum \hbar\omega_{\text{LSPs},l}\hat{b}_{\text{l}}^{\dagger}\hat{b}_{\text{l}}$ describing the quantized LSPs modes $\hat{b}_l$ with resonance frequencies $\omega_{\text{LSPs,l}}$, where $l = 1, 2, \ldots$ labels the mode order (dipole, quadrupole, etc). Furthermore, we consider particles with scale much smaller than wavelength, so that only dipolar LSPs ($l = 1$) is coupled to the cavity field. The third term interaction Hamiltonian then reads $\hat{H}_{\text{I}} = \hbar g_{\text{l}}(\hat{a}^{\dagger} + \hat{a})(\hat{b}_{\text{l}}^{\dagger} + \hat{b}_{\text{l}})$, with g_{l} being the coupling coefficient between the Bloch-SPPs and the dipolar LSPs mode, for convenience, written as $\hat{H}_{\text{I}} = \hbar g(\hat{a}^{\dagger} + \hat{a})(\hat{b}^{\dagger} + \hat{b})$. For the process of $\hbar g\hat{a}^{\dagger}\hat{b}^{\dagger}$ and $\hbar g\hat{a}\hat{b}$ energy is not conserved, so it can be omitted, this is known as the rotating wave approximation (RWA). Thus, the Hamiltonian of the strong coupling system become

$$\hat{H} = \hat{H}_{\text{Bloch - Spps}} + \hat{H}_{\text{LSPs}} + \hat{H}_{\text{I}} = \hbar\omega_{\text{Bloch - SPPs}}\hat{a}^{\dagger}\hat{a} + \hbar\omega_{\text{LSPs}}\hat{b}^{\dagger}\hat{b} + \hbar g(\hat{a}^{\dagger}\hat{b} + \hat{a}\hat{b}^{\dagger}) \ . \tag{S2}$$

5.1 Eigen-energy, hopfield coefficient

Equation (S2) can be transformed into: $\hat{H} = \begin{bmatrix} \hat{a}^{\dagger} \\ \hat{b}^{\dagger} \end{bmatrix}^{\text{T}} \begin{bmatrix} \hbar\omega_{\text{Bloch-SPPs}} & \hbar g \\ \hbar g & \hbar\omega_{\text{LSPs}} \end{bmatrix} \begin{bmatrix} \hat{a} \\ \hat{b} \end{bmatrix}$. Therefore, the eigen-energies of Eq. (S2) can be obtained by solving the following eigen-equation:

$$\begin{bmatrix} \hbar\omega_{\text{Bloch-SPPs}} & \hbar g \\ \hbar g & \hbar\omega_{\text{LSPs}} \end{bmatrix} \begin{bmatrix} \alpha \\ \beta \end{bmatrix} = E_{\pm} \begin{bmatrix} \alpha \\ \beta \end{bmatrix} \ , \tag{S3}$$

here, $E_{\pm}=\dfrac{\hbar(\omega_{\text{Bloch-SPPs}}+\omega_{\text{LSPs}})\pm\sqrt{\Delta^2+4(\hbar g)^2}}{2}$ are the photon energies of upper polariton (UP) and lower polariton (LP) modes, $\Delta=\hbar\omega_{\text{Bloch-SPPs}}-\hbar\omega_{\text{LSPs}}$ is the detuning, where we can define the generalized Rabi frequency of the quantum case as $\sqrt{\Delta^2+4(\hbar g)^2}$, when detuning $\Delta=0$, Rabi frequency $\Omega=2g$. $|\alpha|^2$ and $|\beta|^2$ are the Hopfield coefficients of Bloch-SPPs mode and LSPs mode in UP/LP mode.

5.2 Steady-state solution: emission spectra

Applying Heisenberg equation of motion $\dot{\hat{O}}=\mathrm{i}/\hbar\left[\hat{H},\hat{O}\right]$ to Eq. (S2), the following can be obtained:

$$\begin{cases}\dot{\hat{a}}=\mathrm{i}\left[\omega_{\text{Bloch-SPPs}}\hat{a}^\dagger\hat{a}+\omega_{\text{LSPs}}\hat{b}^\dagger\hat{b}+g(\hat{a}^\dagger\hat{b}+\hat{a}\hat{b}^\dagger),\hat{a}\right]\\ \dot{\hat{b}}=\mathrm{i}\left[\omega_{\text{Bloch-SPPs}}\hat{a}^\dagger\hat{a}+\omega_{\text{LSPs}}\hat{b}^\dagger\hat{b}+g(\hat{a}^\dagger\hat{b}+\hat{a}\hat{b}^\dagger),\hat{b}\right]\end{cases}, \tag{S4}$$

where,

$$\begin{aligned}\dot{\hat{a}}=&\mathrm{i}\left[\omega_{\text{Bloch-SPPs}}\hat{a}^\dagger\hat{a}+\omega_{LSPs}\hat{b}^\dagger\hat{b}+g(\hat{a}^\dagger\hat{b}+\hat{a}\hat{b}^\dagger),\hat{a}\right]\\ =&\mathrm{i}(-\omega_{\text{Bloch-SPPs}}\hat{a}+0-g\hat{b}+0)=-\mathrm{i}\omega_{\text{Bloch-SPPs}}\hat{a}-\mathrm{i}g\hat{b}\,,\end{aligned} \tag{S5a}$$

similarly,

$$\dot{\hat{b}}=-\mathrm{i}\omega_{\text{LSPs}}\hat{b}-\mathrm{i}g\hat{a}. \tag{S5b}$$

Considering loss and optical pumping, Eq. (S4) become

$$\begin{cases}\dot{\hat{a}}=-\left(\mathrm{i}\omega_{\text{Bloch-SPPs}}+\dfrac{\gamma_{\text{Bloch-SPPs}}}{2}\right)\hat{a}-\mathrm{i}g\hat{b}\\ \dot{\hat{b}}=-\left(\mathrm{i}\omega_{\text{LSPs}}+\dfrac{\gamma_{\text{LSPs}}}{2}\right)\hat{b}-\mathrm{i}g\hat{a}+\sqrt{\Gamma_{\text{LSPs,in}}}\hat{b}_{\text{in}}\end{cases}, \tag{S5}$$

where $\hat{b}_{\text{in}}=\hat{b}_{\text{in}}(0)\mathrm{e}^{\omega_{\text{pump}}t}$ are input operators represent the optical pump to Bloch-SPPs and LSPs mode, ω_{pump} is the frequency of the optical pump, $\gamma_{\text{Bloch - SPPs}}$ and γ_{LSPs} are decay rates of the Bloch-SPPs and the LSPs modes, $\Gamma_{\text{LSPs,in}}$ is pump rate to the LSP modes.

To get rid of the time-varying terms, the equations are solved in the rotating frame, where the operators $\hat{O}(t)(\hat{O}=\hat{a}$ and $\hat{b})$ in Eq. (S5) are replaced by $\hat{O}(t)\rightarrow\hat{O}\mathrm{e}^{\mathrm{i}\omega_{\text{pump}}t}$, therefore the time-varying terms can be cancelled

$$\begin{cases}\dot{\hat{a}}=-\left(\mathrm{i}\Delta_{\text{Bloch-SPPs}}+\dfrac{\gamma_{\text{Bloch-SPPs}}}{2}\right)\hat{a}-\mathrm{i}g\hat{b}\\ \dot{\hat{b}}=-\left(\mathrm{i}\Delta_{\text{LSPs}}+\dfrac{\gamma_{\text{LSPs}}}{2}\right)\hat{b}-\mathrm{i}g\hat{a}+\sqrt{\Gamma_{\text{LSPs,in}}}\hat{b}_{\text{in}}(0)\end{cases}, \tag{S6}$$

where $\Delta_{\text{Bloch-SPPs}}=\omega_{\text{Bloch-SPPs}}-\omega_{\text{pump}}$ and $\Delta_{\text{LSPs}}=\omega_{\text{LSPs}}-\omega_{\text{pump}}$.

Set $\dot{\hat{O}}=0$ to obtain the steady-state solutions, $\hat{a}(t\rightarrow\infty)$ and $\hat{b}(t\rightarrow\infty)$:

$$\begin{cases}\left(\mathrm{i}\Delta_{\text{Bloch-SPPs}}+\dfrac{\gamma_{\text{Bloch-SPPs}}}{2}\right)\hat{a}+\mathrm{i}g\hat{b}=0\\ \mathrm{i}g\hat{a}+\left(\mathrm{i}\Delta_{\text{LSPs}}+\dfrac{\gamma_{\text{LSPs}}}{2}\right)\hat{b}=\sqrt{\Gamma_{\text{LSPs,in}}}\hat{b}_{\text{in}}(0)\end{cases}. \tag{S7}$$

Equation (S7) is solved as:

$$\hat{a}(t\rightarrow\infty)=\frac{\begin{vmatrix}0 & \mathrm{i}g\\ \sqrt{\Gamma_{\text{LSPs,in}}}\hat{b}_{\text{in}}(0) & \mathrm{i}\Delta_{\text{LSPs}}+\frac{1}{2}\gamma_{\text{LSPs}}\end{vmatrix}}{\begin{vmatrix}\mathrm{i}\Delta_{\text{Bloch-SPPs}}+\frac{1}{2}\gamma_{\text{Bloch-SPPs}} & \mathrm{i}g\\ \mathrm{i}g & \mathrm{i}\Delta_{\text{LSPs}}+\frac{1}{2}\gamma_{\text{LSPs}}\end{vmatrix}},\quad\text{and}\quad\hat{b}(t\rightarrow\infty)=\frac{\begin{vmatrix}\mathrm{i}\Delta_{\text{Bloch-SPPs}}+\frac{1}{2}\gamma_{\text{Bloch-SPPs}} & 0\\ \mathrm{i}g & \sqrt{\Gamma_{\text{LSPs,in}}}\hat{b}_{\text{in}}(0)\end{vmatrix}}{\begin{vmatrix}\mathrm{i}\Delta_{\text{Bloch-SPPs}}+\frac{1}{2}\gamma_{\text{Bloch-SPPs}} & \mathrm{i}g\\ \mathrm{i}g & \mathrm{i}\Delta_{\text{LSPs}}+\frac{1}{2}\gamma_{\text{LSPs}}\end{vmatrix}}.$$

The total emission is $S(\omega_{\text{pump}})=\gamma_{\text{Bloch-SPPs}}\langle\hat{a}^\dagger\hat{a}\rangle_{t\rightarrow\infty}+\gamma_{\text{LSPs}}\langle\hat{b}^\dagger\hat{b}\rangle_{t\rightarrow\infty}$.

5.3 Time evolution

By solving Eq. (S6) to obtain $\hat{a}(t,\omega_{\mathrm{pump}})$ and $\hat{b}(t,\omega_{\mathrm{pump}})$, the populations of Bloch-SPPs mode and LSPs mode: $\langle\hat{a}^{\dagger}\hat{a}\rangle(t,\omega_{\mathrm{pump}})$ and $\langle\hat{b}^{\dagger}\hat{b}\rangle(t,\omega_{\mathrm{pump}})$ can be obtained.

References

S1. Barredo-Damas S, Lee K, Kirchgeorg R et al. Transparent self-ordered niobium-oxide nanochannel layers formed on conducting glass by total anodization of thin metal films in glycerol/phosphate electrolyte. *ECS Electrochem Lett* **2**, C4–C6 (2013).

S2. Masuda H, Satoh M. Fabrication of gold nanodot array using anodic porous alumina as an evaporation mask. *Jpn J Appl Phys* **35**, L126–L129 (1996).

S3. O'Sullivan JP, Wood GC. The morphology and mechanism of formation of porous anodic films on aluminium. *Proc Roy Soc A Math, Phys Eng Sci* **317**, 511–543 (1970).